Short-term creep and low cycle fatigue unified criterion for a hybridised composite material

Stéphane Gillet, Thomas Jacopin, Sébastien Joannès, Nacera Bedrici, Lucien Laiarinandrasana

▶ **To cite this version:**

Stéphane Gillet, Thomas Jacopin, Sébastien Joannès, Nacera Bedrici, Lucien Laiarinandrasana. Short-term creep and low cycle fatigue unified criterion for a hybridised composite material. International Journal of Fatigue, 2022, 155, pp.106571. 10.1016/j.ijfatigue.2021.106571 . hal-03462858

HAL Id: hal-03462858

https://minesparis-psl.hal.science/hal-03462858

Submitted on 16 Oct 2023

HAL is a multi-disciplinary open access archive for the deposit and dissemination of scientific research documents, whether they are published or not. The documents may come from teaching and research institutions in France or abroad, or from public or private research centers.

L'archive ouverte pluridisciplinaire **HAL**, est destinée au dépôt et à la diffusion de documents scientifiques de niveau recherche, publiés ou non, émanant des établissements d'enseignement et de recherche français ou étrangers, des laboratoires publics ou privés.

Distributed under a Creative Commons Attribution - NonCommercial 4.0 International License

Version of Record: https://www.sciencedirect.com/science/article/pii/S0142112321004229
Manuscript_590e92f55dc4ff3c7308cb237535f0a4

Short-term creep and low cycle fatigue unified criterion for a hybridised composite material

S. Gillet[a,c,*], T. Jacopin[b], S. Joannès[c], N. Bedrici[a], L. Laiarinandrasana[c]

[a] *ESTACA Campus Ouest - Parc Universitaire laval-Changé - Rue Georges Charpak - BP 76121 - 53061 Laval Cedex 9, France*
[b] *ContiTech AVS France - SAS BU Vibration Control - 24, rue Nicolas Joseph Cugnot - 35043 Rennes CEDEX, France*
[c] *MINES ParisTech, PSL University, Centre des Matériaux (CMAT), CNRS UMR 7633, BP 87 91003 Evry Cedex, France*

Abstract

The objective of this work is to determine a low cycle fatigue criterion for a thermoplastic matrix composite reinforced with both short and continuous fibres. The proposed criterion is based on the steady state *creep strain rate* and unifies the results for different fibre orientations, stress ratio, frequency and water content. The criterion is applicable in low cycle fatigue and creep. By means of this criterion, the Monkman-Grant relationship is verified both for creep and low cycle fatigue and offers interesting perspectives for numerical approaches.

Keywords: Hybrid microstructure, Creep-fatigue criterion, Short and continuous fibres, Polyamide, Monkman-Grant relationship

1. Introduction

Thermoplastic matrix composites are increasingly used for transport and mobility applications because they offer an interesting potential for weight

*Corresponding author
Email address: stephane.gillet@estaca.fr (S. Gillet)

© 2021 published by Elsevier. This manuscript is made available under the CC BY NC user license
https://creativecommons.org/licenses/by-nc/4.0/

reduction by replacing metal parts. Short and long fibres reinforced thermoplastic composite materials are now used in structural parts such as clutch pedals [1], engine mounts [2] and fuel rails [3]. The addition of continuous reinforcements using the DynaFib [4] process further improves the mechanical properties and thus the weight reduction potential of these composite materials. Hybridisation of short fibres with continuous fibres in the same material brings innovative design solutions. In the material under consideration, a continuous fibre reinforced thermoplastic (PA6GF60) is overmoulded with a short fibre reinforced thermoplastic (PA66GF50). The prescribed *hybridisation* does not use fibres of different natures, as is generally the case for composites, but relies on the use of two lengths and two diameters of reinforcement through the thickness of the material. In the following we will use the term *hybrid material* to refer to the continuous UD ply covered on both sides with SFRT plies, i.e. the short fibre reinforced thermoplastic plies.

In order to better assess the lifetime of the technical parts made from this *hybrid material*, it is essential to use reliable representative mechanical models to meet all relevant criteria such as part stiffness, strength, durability, impact, noise, vibration and harshness, creep deformation [5]. This work focuses on the Low Cycle Fatigue (LCF) of the *hybrid material*. The hydrothermal environmental variables, as well as the microstructure induced by the manufacturing process are important parameters to take into account [6, 7, 8, 9]. This paper aims to define a LCF criterion for the whole *hybrid material* as well as for the SFRT separately while providing a relationship with the creep loading. This work is part of a more global study, which consists of experimentally identifying the damage mechanisms

in the LCF domain, both on macroscopic and microscopic scales.

The fatigue response of polyamide 6.6 (PA66) SFRT materials has been studied mainly in the field of High Cycle Fatigue Domain (HCF), beyond 10^3 cycles. For HCF, several authors have shown that the *cyclic creep strain rate* criterion seems to be relevant to unify fatigue curves of such materials. Horst and Spoormaker [10] showed a linear correlation between the fatigue life and the *cyclic creep strain rate*. Bernasconi and Kulin [11] investigated the influence of frequency on the fatigue behaviour of a polyamide 6 (PA6) SFRT. They expressed the relationship between temperature rise, applied stress, and *cyclic creep strain rate* in terms of a parameter derived from the Larson-Miller [12] steady creep parameter. Seignobos [13] showed that *cyclic creep strain rate* unifies tests at different temperatures for a PA66 reinforced with 30 wt% short glass fibres. Rolland [9] was able to unify the fatigue results on a PA66GF30 at 50 % RH for load ratios ranging from 0.1 to 0.7 with *cyclic creep strain rate* as criterion. Raphael et al. [14] proposed two *cyclic creep strain rate* based criteria; one of the two introducing anelastic energy, to better take into account mean stress effect and unify fatigue life predictions within scatter bands of factor two. Finally, Santharam et al. [15] evaluated the accuracy of many of the literature criteria on a large database that took into account the influence of orientation (0°, 45° and 90°), stress ratio (-0.5 to 0.7) and the position of the test temperature in relation to the glass transition temperature (T_g). They showed that criteria based on *cyclic creep strain rate* gave very good results to unify fatigue tests except for negative stress ratios. Finally, they proposed two unified criteria based on *cyclic creep strain rate* and mean stress in order to unify the whole test database (over 90 % of the database was unified within a scatter band

of three).

All these studies have been carried out mainly in the field of HCF with materials with free faces. The first purpose of this paper is to unify results in the LCF domain for SFRT with a criterion based on *cyclic creep strain rate*. In the hybrid material under study, the UD reinforcement constrains the SFRT at the interface between the two materials (Figure 1). Crack growth mechanisms observation of the *hybrid material*, at different scales, allowed the determination of a damage chronology that highlights the main influence of the SFRT in the failure. Figure 1 (a) presents the crack formation on the SFRT surface during the last fatigue cycle of the *hybrid material*, 2.7 ms before the strength loss. On most of the fatigue specimens, a crack appeared in the SFRT shortly before the failure, this crack seemed to propagate towards the face with the UD reinforcement and then led to the failure of the material. These observations were also made on a microscopic scale using fast X-ray tomography. Figure 1 (b) illustrates the cracks in SFRT on a scan performed during the last cycle. This information was obtained in a specific campaign carried out with synchrotron radiation. The local approach with micro-CT observation is outside the scope of this article which focuses on the global approach. This results shows that SFRT has a major role in the failure of *hybrid material*. This leads to the second purpose of this paper: apply this criterion to the *hybrid material* studied, consisting of an SFRT constrained by a UD reinforcement.

Concerning creep loading, links between the minimum or steady state *creep strain rate* and time to failure (t_f) are usually represented in terms of Monkman-Grant relationships [16, 17]. The *creep strain rate* was first introduced as criterion to predict creep failure times for metals. It has been

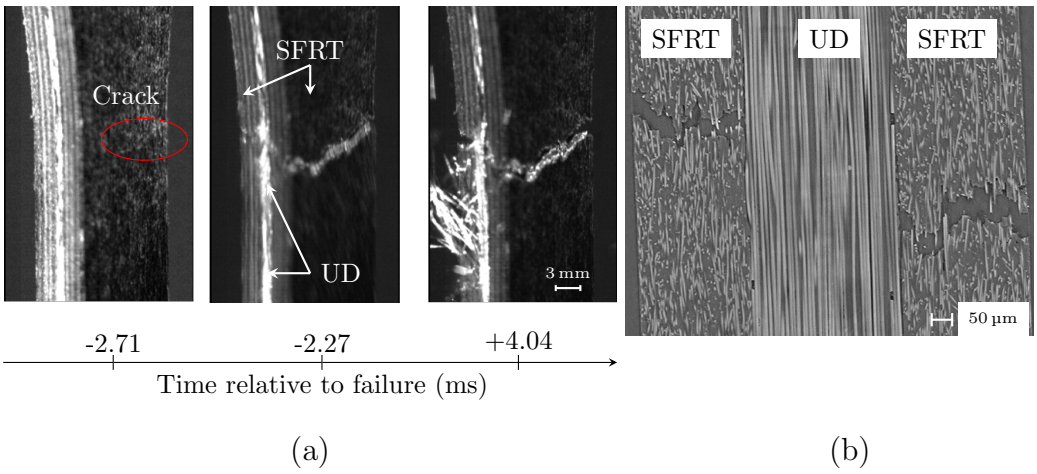

Figure 1: (a) High speed camera image captures near failure time (strength loss) during LCF test. (b) In-situ LCF test with fast X-ray tomography: scan at failure.

demonstrated by several authors [18, 19] that this empirical relationship is a powerful and reliable way to predict the long-term material lifetime from short-term tests over a wide range of temperatures and stress fields. Despite its simplicity it has succeeded to predict failure times, with some accuracy [20], for a wide range of materials, including also polymers [21, 22] or adhesive anchor systems [23]. The last objective is to relate fatigue to creep through this criterion base on *creep strain rate*.

In order to achieve these objectives, the paper is organised as follows: the first section describes the methodology for determining the criterion in the fields of fatigue and creep. The second section presents the material and the specimens used in the papers. In the third and last section the experimental approach and results are discussed. In this section, the influence of different parameters, such as microstructure and moisture absorption on LCF and creep results is highlighted. Then, in the last section, the *cyclic creep strain rate* criterion is evaluated in the LCF domain, first on the SFRT, then on

the whole *hybrid material*. Finally, the *cyclic creep strain rate* is related to time instead of the number of cycles to failure in the case of fatigue loading in order to unify the results obtained in fatigue and creep.

2. Methodology

In the present work, all the scheduled tests were load controlled. This kind of loading is specific for creep tests for which the material response is generally analysed in terms of creep displacement or creep deformation/strain. For fatigue tests with an imposed load, a similar analysis is attempted here, by contrast with many results in the literature, with stress approach [24, 13] or energetic approach [25, 26]. In the case of load imposed tests, the strain is the dual variable of the imposed stress field. As a result, the strain and the strain rate have the advantage of being "material responses".

2.1. Data reduction for creep tests

In the case of creep test (steady load) the evolution of the creep strain (ε_c) as a function of creep usage ratio is represented in Figure 2 (a).

In this figure, the creep usage ratio t/t_f is introduced as:

$$\text{Creep usage ratio} = \frac{t}{t_f} \tag{1}$$

with t, the creep time i.e. the time running after the end of the loading stage; and t_f, the creep time to failure. In order to identify the three creep stages, the evolution of the *creep strain rate* is plotted by using the time-derivative of Figure 2 (a). A representative result is illustrated in Figure 2 (b), where:

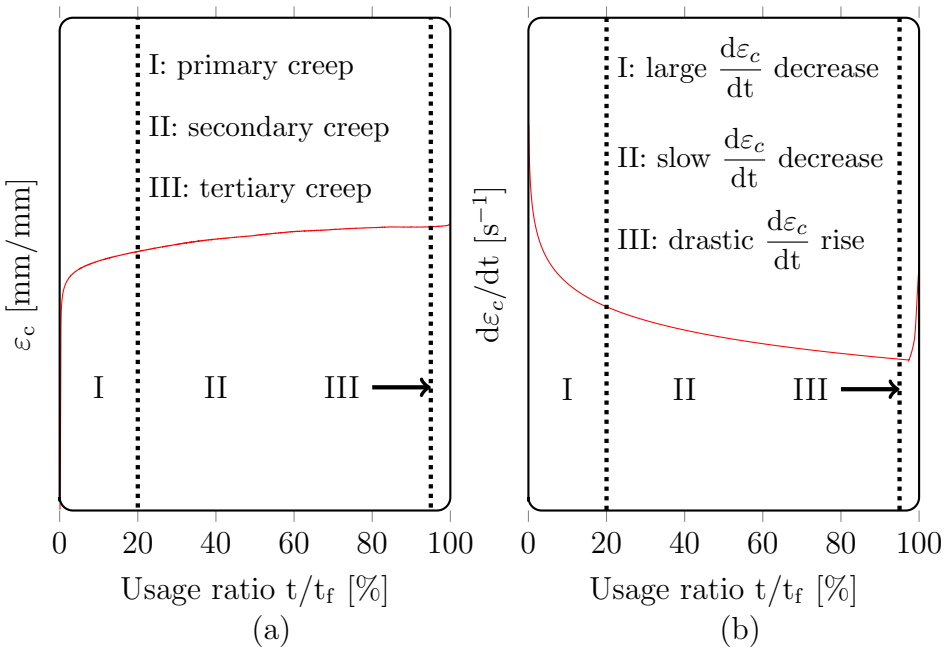

Figure 2: Creep test. Creep strain (a) and creep strain rate (b) as a function of creep usage ratio.

- a primary creep stage I, between 0 % and 20 % of usage ratio, characterised by transient creep with high decreasing rate of the *creep strain rate*;
- a secondary creep stage II, between 20 % and 95 %-100 % of usage ratio, characterised by a slow decreasing rate or an assumed stabilised *creep strain rate*;
- a tertiary creep stage III, near 95 %-100 % of the usage ratio, characterised by a rapid increase of the *creep strain rate*.

Creep fracture in uniaxial tension under constant stress has been described by the Monkman–Grant relationship [16] which states that the frac-

ture of creep deforming materials is controlled by the minimum *creep strain rate*.

Monkman-Grant relationship [16]:

$$\frac{\mathrm{d}\varepsilon}{\mathrm{d}t} t_f^n = C \tag{2}$$

where C is referred to as the Monkman–Grant constant and n value is typically about 1.0. C lies between 0.05 and 0.5 for metallic material [16]. This type of phenomenological relationship is based on the observation that strain rate is the macroscopic demonstration of the cumulative creep damage [27, 17]. The Monkman-Grant relationship is used in the field of metallic materials to estimate the temperature creep resistance. This relationship should give a slope of -1 on a log-log plot of minimum creep strain rate versus time to failure regardless of temperature or applied stress for a particular material. It then becomes simple to predict a time to failure by measuring the minimum creep strain rate at a given stress and temperature.

2.2. Proposition for data reduction for fatigue tests with load control

Following [11, 8, 14, 9, 15, 13] for fatigue tests with a controlled load, the *cyclic creep strain rate* is considered here. It was determined in different ways depending on the authors: from the evolution of the minimum or maximum strain in each cycle [11, 8], or from the mean strain [14, 9, 15]. Selles [28] proposed a calculation of the *cyclic creep strain rate* at peak and troughs, i.e. from the minimum and maximum strain, considering two different initial reference lengths by adding each time, respectively, the minimum and maximum strain of the first cycle.

Figure 3 (a) describes the hysteresis loop at a given cycle where ε_{min}, ε_{max} and the mean strain ε_{m} are defined. The *cyclic creep strain rate* is

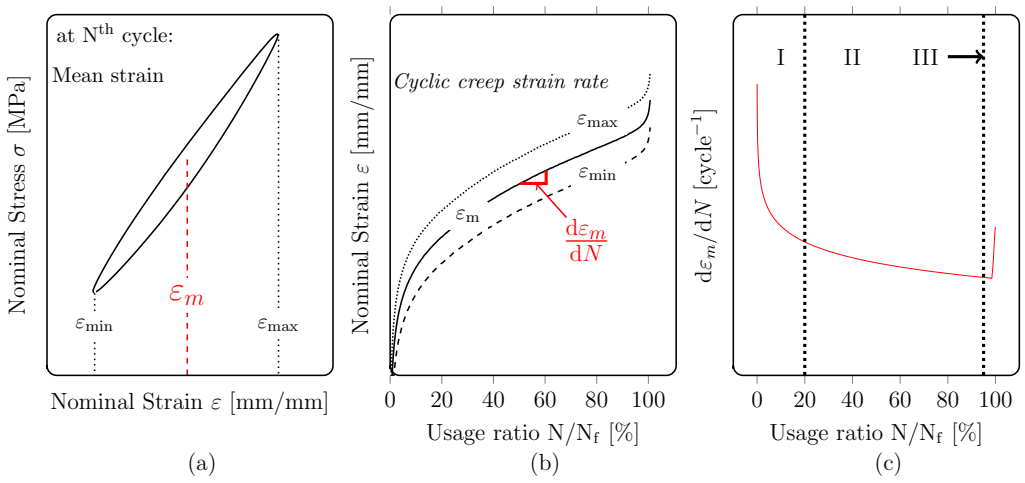

Figure 3: (a) Nominal stress-strain fatigue at a given cycle. (b) Maximum, Mean and minimum strain evolution during fatigue test and *cyclic creep strain rate* expression. (c) *Cyclic creep strain rate* as a function of fatigue usage ratio during fatigue test. The mean strain evolution in fatigue is typical of that obtained in creep with three distinct zones.

obtained by deriving ε_{m} with respect to the current number of cycles (Figure 3 (b)):

$$\textit{Cyclic creep strain rate} = \frac{\mathrm{d}\varepsilon_m}{\mathrm{d}N} \tag{3}$$

Note that in the latter figure, the fatigue *usage ratio* was also introduced as:

$$\text{Fatigue usage ratio} = \frac{N}{N_f} \tag{4}$$

with N the fatigue current cycle number and $\mathrm{N_f}$ the number of cycle to failure.

Plotting the *cyclic creep strain rate* with respect to the fatigue usage ratio (Figure 3 (c)) allows the analogy between the creep and fatigue stages to be illustrated. Indeed, the primary, secondary and tertiary creep stages in Figure 3 (c) could also be identified in Figure 2 (b).

The practice in the creep tests is to select a stabilised value of the creep strain rate for a given test. Typically the minimum creep strain rate corresponding to the secondary - assumed to be stationary - creep stage is chosen. For fatigue tests with load control, the same approach can be applied to the *cyclic creep strain rate*. For Horst and Spoomaker [8], it was calculated by averaging over the secondary creep stage, whereas the criterion was the *cyclic creep strain rate* at mid-life in the references [14, 9]. In this paper, the fatigue criterion is calculated by averaging the *cyclic creep strain rate* between 30 % and 90 % of the lifetime within the secondary creep stage. For the sake of simplicity, it will be named as the *cyclic mean strain rate* in the following. The criterion is written as follows and will be calculated for each test:

$$\textit{Cyclic mean strain rate criterion} = \overline{\frac{\mathrm{d}\varepsilon_m}{\mathrm{d}N}} \tag{5}$$

Criterion for creep test is determined in the same way by averaging the *creep strain rate* between 30 % and 90 % of the lifetime within the secondary creep stage.

$$\textit{Creep mean strain rate criterion} = \overline{\frac{\mathrm{d}\varepsilon_c}{\mathrm{d}t}} \tag{6}$$

The relationship between the number of cycles and the time is made through the frequency:

$$t = \frac{N}{f} \tag{7}$$

Cyclic mean strain rate criterion is written as follows in time domain:

$$\textit{Cyclic mean strain rate criterion} = \overline{\frac{\mathrm{d}\varepsilon_m}{\mathrm{d}t}} = f\overline{\frac{\mathrm{d}\varepsilon_m}{\mathrm{d}N}} \tag{8}$$

3. Material and specimens

3.1. Material

The UD reinforcement is a PA6 reinforced by 60 wt% of continuous glass fibres with a diameter of about 20 µm; this material is referred to as UD PA6. The wrapping material is a PA66 matrix reinforced by 50 wt% of short glass fibres with an average length and diameter of about, respectively, 250 µm and 11 µm; this material is named as SFRT.

The *hybrid material* plates were processed, with the same mould, in three steps:

- a three plies lay-up of UD PA6 was manufactured using an automated fibre placement (AFP) to obtain a reinforcing plate of (150 mm×150 mm×0.9 mm);
- a first overmoulding of SFRT was performed by injection on one side of the reinforcing plate, for which, the thickness was 3 mm;
- a second overmoulding of SFRT followed on the opposite side of the reinforcing plate (3 mm thickness) so as to obtain a plate with the UD PA6 centred at mid-thickness (Figure 4 (c)).

For each overmoulding, the Mould Flow Direction (MFD) was parallel to the direction of the UD continuous fibres. The obtained *hybrid material* consisted of an injection moulded plate with characteristic lengths of 300 mm×150 mm×6.9 mm (Figure 4).

3.2. Specimens and microstructure

The specimens were cut out from the aforementioned *hybrid plate*. The dimensions of the specimens are detailed in (Figure 4 (a)). In addition, the

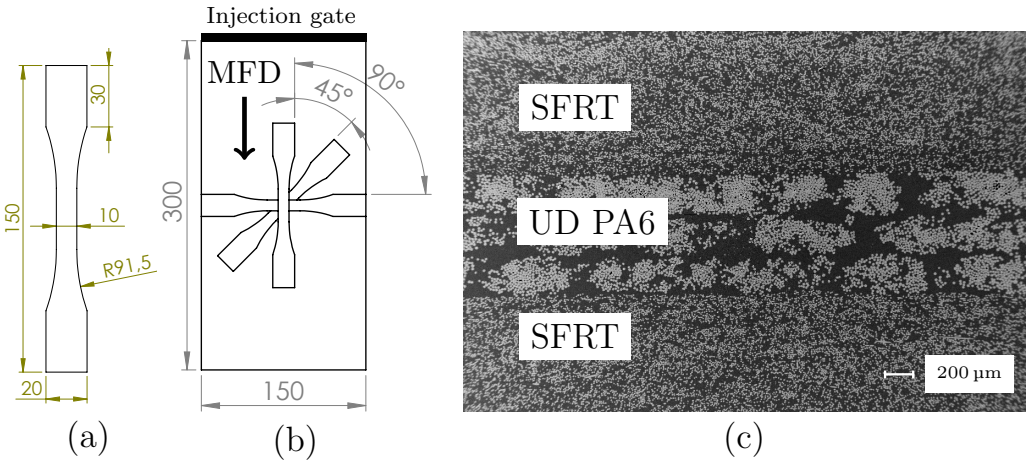

Figure 4: (a) Specimen dimensions (mm). (b) Mould plate dimension (mm) and cutting sample orientations. (c) *Hybrid material*: UD plies overmoulded by SFRT (SEM).

same specimen geometry was used to study the sole SFRT material with a thickness of 3 mm. The injection gate is a cylinder positioned at one end across the width of the plate (Figure 4 (b)). According to the MFD, three specific directions θ (0°, 45°, 90°) were studied.

Moreover, the injection process leads to heterogeneity in the fibre orientations, through the thickness as well as the width of the mould plate. The edges of the plate, over a distance of approximately 20 mm, exhibit a fibre orientation predominantly along the MFD (Figure 5 (b)).

When moving towards the centre of the plate (Figure 5 (c)) a skin/core effect [7, 8, 29, 30] is observed. The specimens extracted from the middle of the plate show a core thickness of about 450 µm, i.e. 15 % of the thickness of the SFRT. This allows an investigation on the effect of the microstructure of the specimens extracted at 0° i.e. in MFD from six positions across the width (Figure 5):

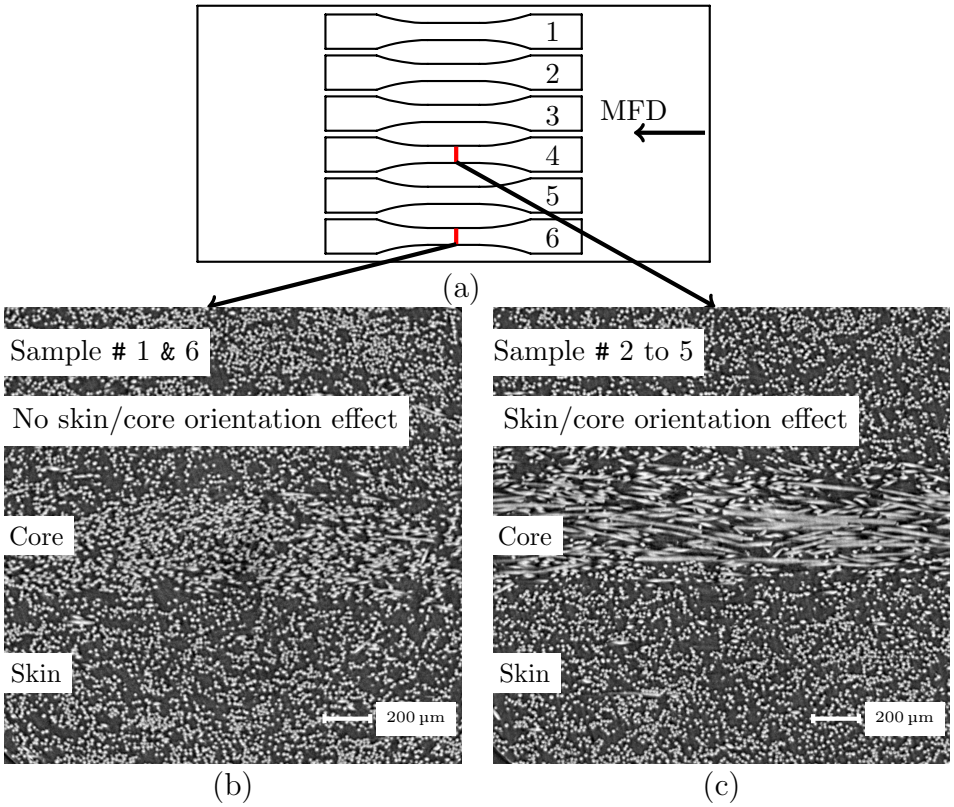

Figure 5: Influence of edge effect on the SFRT microstructure specimen. (a) 0° samples cutting place on moulded plate. (b) X-ray tomography image, specimens taken from the edge (numbers 1 and 6) with fibres mostly oriented along the MFD at the edge. (c) X-ray tomography image, specimens taken from the plate center (numbers 2 to 5) with skin/core orientation effect.

- "homogeneous" and oriented along the MFD for edge specimens (numbers 1 and 6);
- and with a skin/core effect for specimens cut out from the centre of the plate (numbers 2 to 5).

The shape of the specimens was defined so as to maximise the probability

of failure along the gauge length during a tensile test. This was done experimentally by taking specimens of different shapes and performing tensile tests [31].

3.3. Samples conditioning

Prior to the testing, all specimens were conditioned at a given relative humidity (RH) as follows:

- 0 % RH: ventilated oven at 80 °C until mass stabilisation.
- 50 % RH: according to the ISO1110 standard. Specimens are placed at 62 % RH and 70 °C in climatic chamber until mass stabilisation. They are then placed at 50 % RH and 23 °C for two weeks.
- 80 % RH: Specimens are placed at RH=80 % and 70 °C in climatic chamber until mass stabilisation. They are then placed at 80 % RH and 23 °C for two weeks.

Kettle [32] showed that the consequence of relative humidity is the decrease of the glass transition temperature (T_g) of polyamides. In order to investigate the influence of water content on the SFRT, Tg measurements were carried out on the SFRT of the study for the three conditioning mentioned above. Table 1 presents for each conditioning, the water concentration and the T_g for the SFRT.

Increasing the relative humidity from 0 % RH to 80 % RH leads to a reduction of T_g from 66 °C to 0 °C. At 0 % RH the T_g is 21 °C i.e. near the test room temperature T_{test} (23 °C). These different water content conditions allow the influence of the relative position of the T_g with respect to the T_{test}

RH (%)	**C** (%)	T_g (°C)
0	0	66
50	1.5	21
80	2.35	0

Table 1: Influence of relative humidity for PA66GF50 on T_g. RH: material relative humidity, C: water concentration. 50 % RH water content induced a T_g near test room temperature (23 °C). DMA 50N Metravib in tension a=10 µm, f=1 Hz, temperature ramp=2 °C min^{-1}.

to be studied. For SFRT at 0 % RH ($T_{test} < T_g$), at 50 % RH ($T_{test} \approx T_g$) and at 80 % RH ($T_{test} > T_g$). Before the tests, the conditioned specimens were stored in vacuum bags so as to prevent any change in their water content. The maximum duration of this storage was one year before testing. Mass measurements after one year on samples conditioned at 0 % RH and stored in vacuum bags in an environment at 23 °C and 50 % RH showed a water content recovery of 0.2 % by mass. This percentage is generally that of the dry samples as they come out of the mould. It was then assumed that the samples conditioned at 50 % RH and 80 % RH and stored under vacuum, for an equivalent period of time, did not show a variation in water content of more than 0.2 % by mass.

4. Experiments

4.1. Experimental procedure

This section deals with fatigue and creep tests carried out on both SFRT and the *hybrid material*. As the tests were under load control, the focus will

be on the *cyclic creep strain rate*. All the tests were performed on an INSTRON 8801 servo-hydraulic fatigue machine. The material response was then analysed by measuring the extension of the specimens by using an extensometer with a gauge length of 12.5 mm. In some cases this measurement was duplicated with strain gauges or Digital Image Correlation (DIC) measurements on the opposite side. The room temperature was maintained at 23 °C with an ambient humidity close to 50 % RH. It is assumed that the water content in the samples remained constant during the tests. This was checked by mass measurements on control samples. Additionally, in some cases the temperature on the surface of the specimen was measured thanks to a Cedip Titanium infrared thermal camera during the fatigue tests. The purpose was to control the heat build up. For the tests with the *hybrid material* a Photron high-speed camera was also used to visualise the failure period with a frame rate of fifty thousand images per seconds. The basic tests conditions were as follows:

- Imposed load under LCF domain ($N_f < 10^4$ cycles to failure);
- Load ratio: $R_\sigma = 0$;
- Frequency: 1 Hz;
- Environmental conditions: 23 °C; 50 % RH;
- Water content: 50 % RH (ISO 1110).

The sensitivity of the materials response with respect to the frequency, the relative humidity, the positive load ratio and the orientation was further investigated. To this end, additional tests were carried out at 23 °C namely:

- fatigue tests with various conditions in terms of water content (0 % RH and 80 % RH), frequency (0.5 Hz, 2 Hz and 4 Hz) and load ratio (0.2, 0.5 and 0.8);
- creep tests with three water contents (0 % RH, 50 % RH and 80 % RH) and three orientations (0°, 45° and 90°).

The Table 2 summarises the test program.

Test	Material	Test conditions				Test $N_{o.}$
		RH (%)	θ (°)	f (Hz)	R_σ	
LCF	SFRT	0, 50, 80	0, 45, 90	0.2, 1, 2, 4	0, 0.2, 0.5, 0.8	335
LCF	*Hybrid*	50	0	1	0	39
Creep	SFRT	0, 50, 80	0, 45, 90	-	-	50

Table 2: Tests configurations for LCF and creep. Conditions of fatigue tests: water contents, orientations, frequency and load ratios. Conditions of creep tests: water contents and orientations. Tests $N_{o.}$ indicates the number of tests performed.

4.2. Experimental results

The experimental results are displayed using diagrams constituted of the engineering stress – related to the controlled load – versus the time or cycle to failure. This allows the sensitivity of the lifetime criterion in terms of time or number of cycles to failure, according to the prescribed parameters to be investigated, to be highlighted. The stress values are normalised by an arbitrary constant for confidentiality reasons.

4.2.1. Creep tests : S-T curves

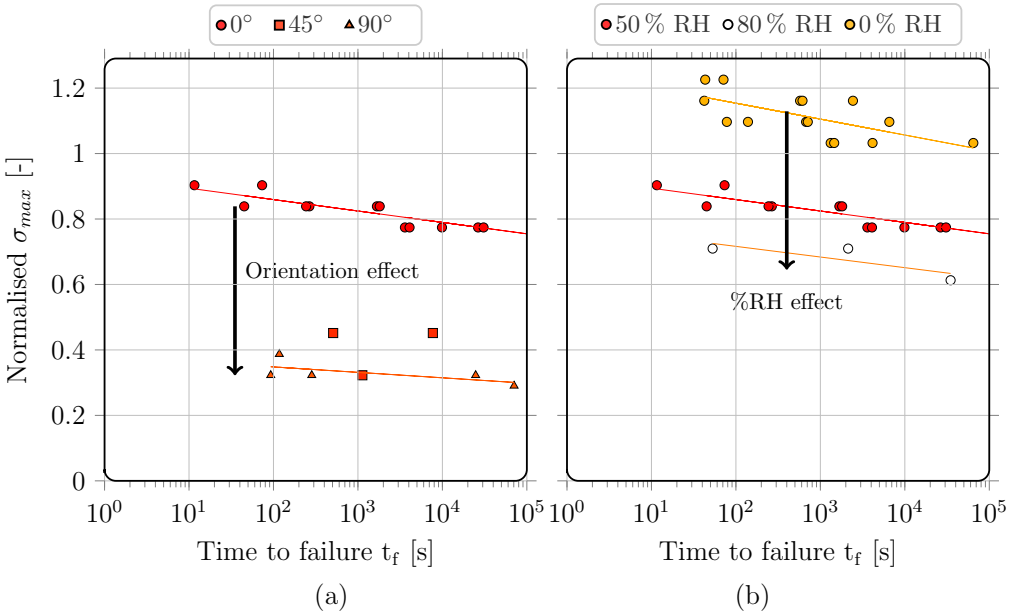

Figure 6: SFRT S-T creep curves. (a) Orientation influences at 50 % RH. (b) Water content influences at 0°.

Figure 6 presents the normalised imposed stress ($\sigma_{\max}$) as a function of the creep time to failure (t_f) named as S-T curves. It is observed that S-T curves are rather "flat" and provide a large scatter for any given stress. For the sake of clarity, test results at 50 % RH are selected in Figure 6 (a) so as to highlight the effects of the orientation. The black arrow indicates the trends of S-T curves when the orientation is increased from 0° to 90°. The effects of the relative humidity is illustrated in Figure 6 (b) where the sample orientation is fixed at 0° for three values of RH: 0 %, 50 % and 80 %. The black arrow shows that the higher the RH value, the lower the S-T curves. These two results are not so common on SFRT in the literature, which focuses on creep-fatigue interaction [33, 34, 35] or on the effect of

temperature [36, 35].

4.2.2. Fatigue tests: S-N curves

The Figures 7 to 9 present Wöhler curves by plotting the maximum normalised imposed stress ($\sigma_{\max}$) as a function of the number of cycle to failure (N_f) named as S-N curves. As already mentioned, the stress values are normalised by an arbitrary constant for confidentiality reasons. Figure 7 shows the S-N curves plotted at R_σ=0, 1 Hz and 50 % RH. The results for the SFRT are presented for three orientations. For *hybrid material*, specimens are oriented at 0°.

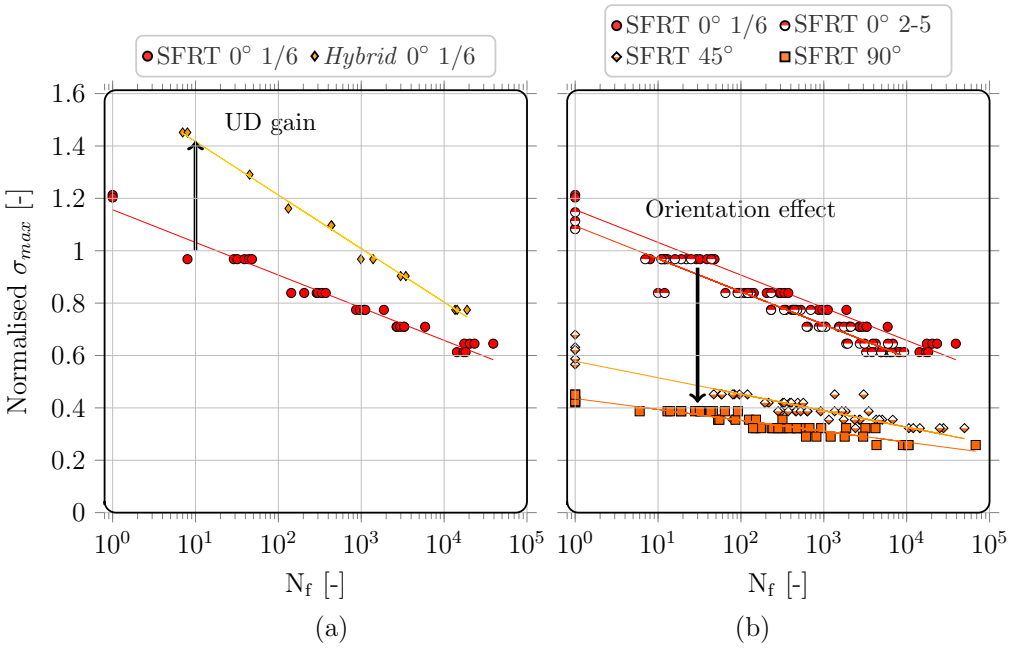

Figure 7: S-N Curves. (a) UD contribution. (b) Orientation influence. R_σ=0, 1 Hz and 50 % RH.

Test results at 0° are selected in Figure 7 (a) so as to highlight the effects of the addition of continuous reinforcement. The black arrow indicates

the trend of S-N curves when UD P6 is associated to SFRT in the *hybrid material*. This shows a clear increase of the fatigue strength. Figure 7 (b) presents the strong influence of fibre orientation for SFRT. For any given applied stress, specimens oriented at 0° have a higher number of cycle to failure than in the other directions. The black arrow indicates the trends of S-N curves when the orientation is increased from 0° to 90°. This has already been reported in the literature as in Horst and Spoormaker [8] and Bernasconi et al. [7] papers. Figure 7 (b) also shows that the 0° test specimens taken from the edges (numbers 1 and 6) have a higher S-N curve than those taken from the centre (numbers 2 to 5). This is a consequence of the heterogeneity of microstructure with predominantly oriented fibres along MFD at the edge and a skin-core effect in the plate center (Figure 5).

In order to extend the SFRT experimental database, further tests were carried out by varying the frequency from 0.5 Hz to 4 Hz, the stress ratio from 0 to 0.8 and the water content from 0 % RH to 80 % RH.

Figure 8 shows the influence of water content and stress ratio on fatigue lifetime. In Figure 8 (a) the data is selected at 0°, 1 Hz and $R_\sigma = 0$ with the aim of showing the water content effect. The fatigue strength decreases with the water content level. The black arrow then indicates trends of S-N curves when the water content is increased from 0 % RH to 80 % RH. Similar results were observed in the literature [6, 37, 9, 15]. The water content modifies the glass transition temperature (Tg) [32, 38]. In this case at 0 % RH $(T_{test} - T_g) < 0$ and at 80 % RH $(T_{test} - T_g) > 0$ (Table. 1). This leads to a decrease in modulus and mechanical strength at 80 % RH. The effects of the load ratio is illustrated in Figure 8 (b). R_σ influence appears from 10^2 to 10^3 cycles, with a slope change, and then the fatigue

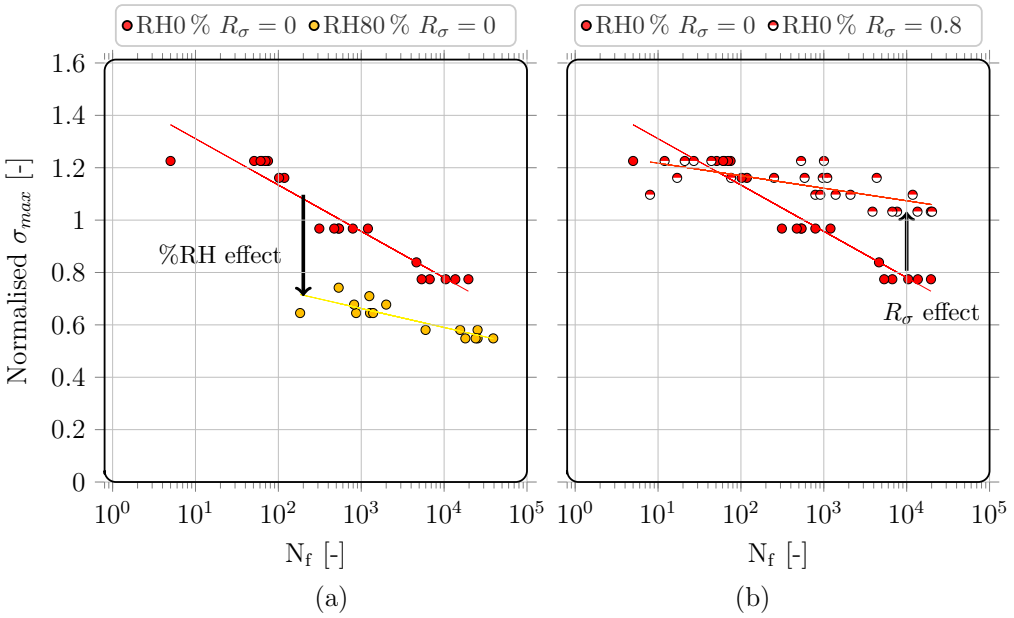

Figure 8: SFRT S-N Curves at f=1 Hz and 0°. (a) Influence of water content at $R_\sigma = 0$. (b) Influence of R_σ at 0 % RH.

strength increases with R_σ. This has been highlighted in HCF domain with the papers of Mallick and Zhou [39] on PA66GF30 and Santharam et al. [15] on PA66GF50. Kanters et al. [5, 40] on PA66GF50 also highlighted the change in slope curve and the R_σ influence from 10^2 to 10^3 onwards for $1 > R_\sigma > 0$. In the LCF domain, the frequency has practically no effect on the SFRT fatigue strength between 0.5 Hz to 4 Hz (Figure 9) with a T_g equal and superior to the test room temperature.

4.2.3. Attempt to compare creep and fatigue curves

In this subsection, an attempt is made to compare the Wöhler like curves in fatigue and in creep. To this end the maximum normalised imposed stress (σ_{max}) is plotted against the time to failure. For fatigue results the relationship between N_f and t_f is through the frequency.

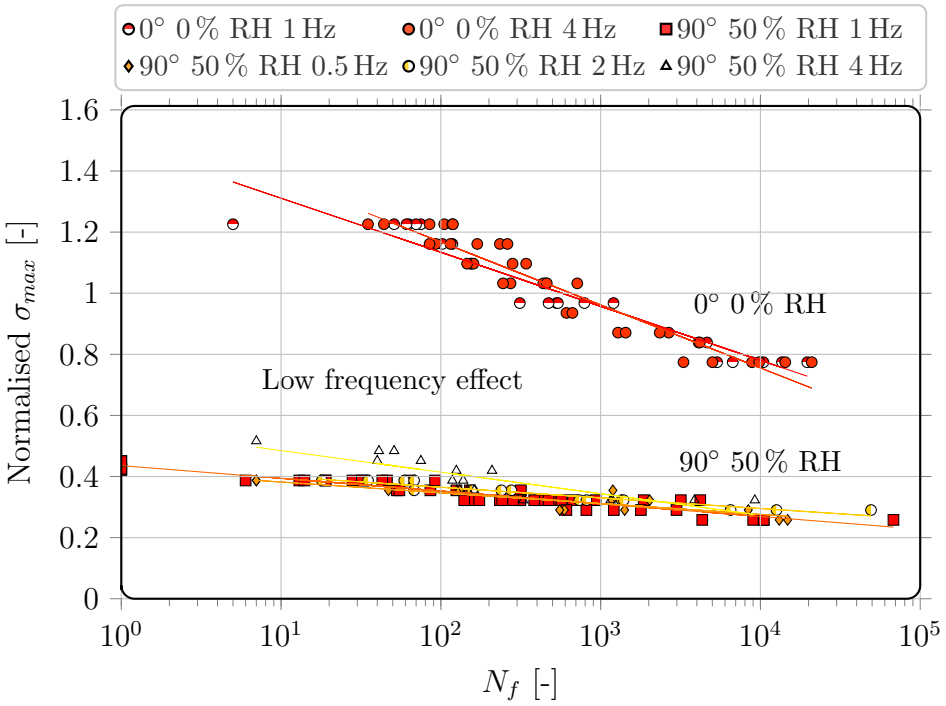

Figure 9: SFRT S-N Curves. Frequency influence.

$$t_f = \frac{N_f}{f} \tag{9}$$

Figure 10 shows comparison between LCF and creep results in the time domain.

There are similarities between creep and LCF results for tests conducted at 45° and 90°. At the same imposed stress, for LCF or creep, the time to failure is relatively close. The difference is clearer for 0° orientation. Note that the creep test can be similar to a fatigue test with a $R_\sigma = 1$.

In conclusion, the creep and LCF test conditions (fibre orientations, water content and R_σ) lead to a wide range of creep and fatigue strengths. For a given applied stress, depending on the test conditions, the range of

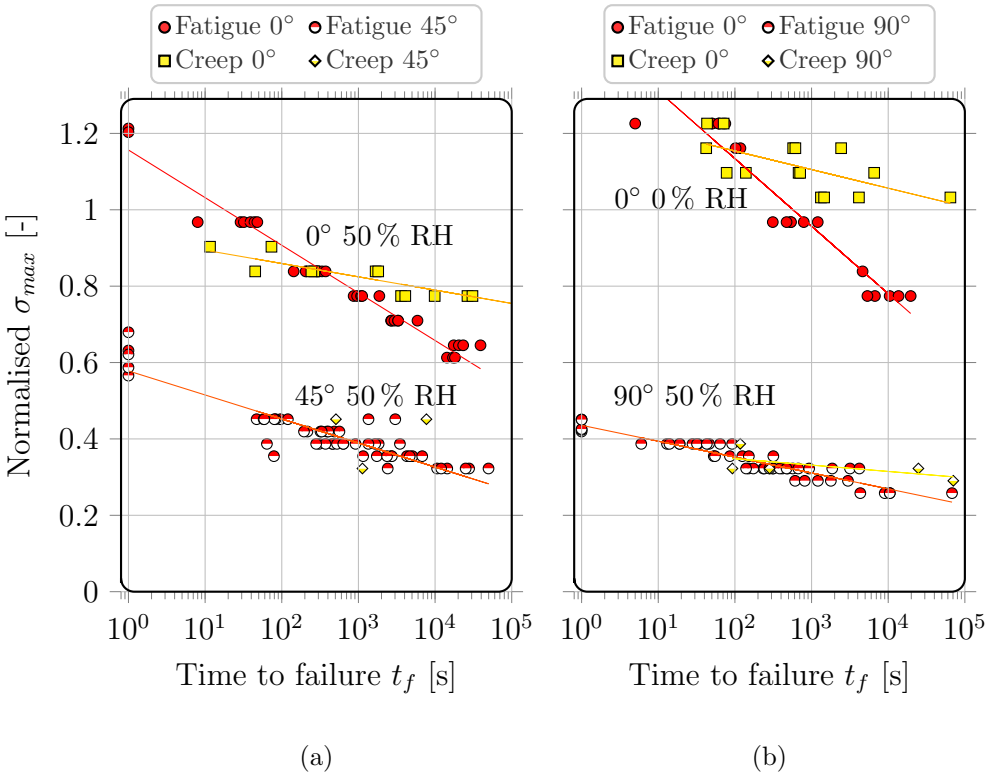

Figure 10: SFRT S-T curves. Comparison between creep and LCF tests.

the creep (resp. fatigue) strengths goes from null up to 10^4 seconds (resp. cycles).

5. Discussion: proposition for creep/fatigue criterion

The objectives of the criterion are to unify:

- Fatigue results for SFRT and *hybrid material*;
- Fatigue and creep SFRT result.

The principle of determining the criterion is set out in section 2.

5.1. Fatigue Criterion

Instead of using σ_{max}, the curves are plotted with the *cyclic mean strain rate* criterion in ordinate. Figure 11 shows results obtained with *cyclic mean strain rate* criterion as a function of the number of cycles to failure N_f. Data is taken from tests carried out on the SFRT from three orientations at 50 % RH, $R_\sigma = 0$ and 1 Hz.

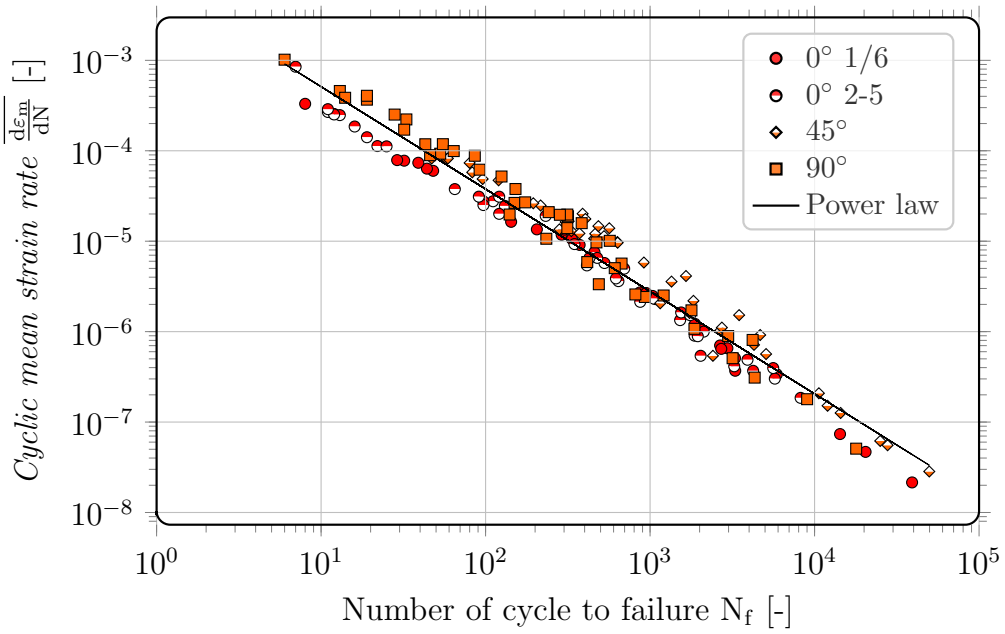

Figure 11: *Cyclic mean strain rate* criterion evolution as a function of number of cycle to failure N_f for PA66GF50, 50 % RH, $R_\sigma = 0$, 1 Hz.

Cyclic mean strain rate criterion allows unification of data according to the fibre orientations. This result can be found in other research work already mentioned [41, 15].

The relationship between the number of cycles to failure and the *cyclic mean strain rate* criterion is written using a power law:

$$\overline{\frac{\mathrm{d}\varepsilon_m}{\mathrm{d}N}} = AN_f^k \tag{10}$$

The calculated lifetime can then be written as follows:

$$N_{fcal} = B\left(\overline{\frac{\mathrm{d}\varepsilon_m}{\mathrm{d}N}}\right)^p \tag{11}$$

with :

$$B = A^{-\frac{1}{k}} \quad \text{and} \quad p = \frac{1}{k}$$

where B, k, A and p are material parameters.

5.1.1. Power law parameters identification

Parameters identification is carried out on a limited panel of 158 SFRT tests at 50 % RH, $\mathrm{R}_\sigma = 0$ and 1 Hz for the three fibre orientations (Results related to Figure 11). The confidence interval at a 95 % confidence level is determined with a random 3000 bootstrap re-sampling [42].

$$A = 6.9 \times 10^{-3} \pm 1.7 \times 10^{-3} \ ; \ k = 1.13 \pm 3.7 \times 10^{-2}$$

$$B = 1.24 \times 10^{-2} \pm 4.5 \times 10^{-3} \ ; \ p = -8.83 \times 10^{-1} \pm 2.8 \times 10^{-2}$$

To determine the criterion accuracy, the ratio $\mathrm{N_{fcal}}/\mathrm{N_{fexp}}$ is plotted as a function of *cyclic mean strain rate* criterion on Figure 12. $\mathrm{N_{fcal}}$ is the estimated lifetime using Eq. (11). $\mathrm{N_{fexp}}$ is the experimental lifetime. Scatter bands of factor two and three are marked in dashed and dotted lines respectively. The criterion unifies the identification database results with 95 % of estimated lifetimes within a scatter band of factor two and 100 % within factor three (Table 3). In the following, the estimated lifetimes are determined with this identification on this restricted database.

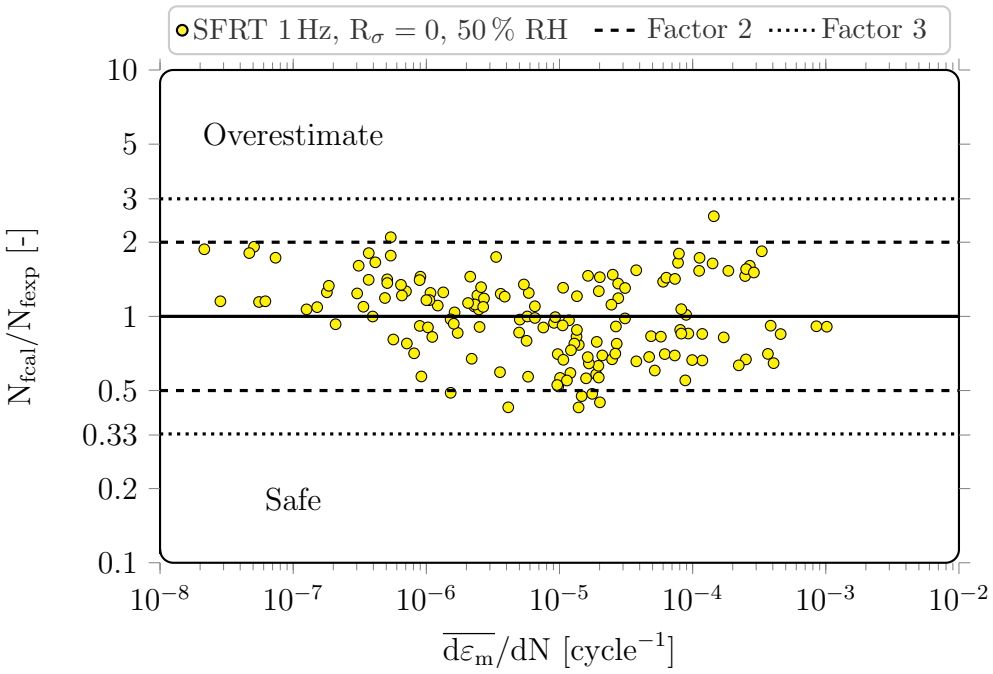

Figure 12: Criterion precision. N_{fcal} estimated using Eq. 11. SFRT for 3 orientations at 1 Hz, $R_\sigma = 0$, 50 % RH tests. Scatter bands of factor two and three are marked in dashed and dotted lines respectively.

5.1.2. Extrapolation to other SFRT test conditions and hybrid material

Figure 13 shows SFRT results obtained on an extend experimental database by varying:

- Fibre orientations (0°, 90° and 45°);
- R_σ (0, 0.2, 0.5 and 0.8);
- Water content (0 % RH, 50 % RH and 80 % RH);
- Frequency (0.5 Hz, 1 Hz, 2 Hz and 4 Hz).

Fifteen different configurations were carried out for a total of 335 tests. The criterion unifies the SFRT database results with 92 % of estimated lifetimes within a scatter band of factor two and 100 % in factor three (Table 3). The criterion therefore unifies the results for SFRT in the LCF domain. Concerning *hybrid material* the estimated lifetime is globally over-estimated with a offset visible in Figure 13. 82 % of estimated lifetimes within a scatter band of factor two and 100 % in factor three (Table 3). This is rather a satisfactory estimation considering that the identification is made on the SFRT only. This again shows that SFRT has a major role in the failure of *hybrid material*. Despite the SFRT having a constrained face in the *hybrid material*, the criterion identified on samples without any constrained face is applicable.

5.2. Criterion extension to creep

As mentioned in section 2, the curves for creep strain (as a function of time) and fatigue strain (as a function of the number of cycles) follow the same evolution. In order to link fatigue and creep, all curves are expressed

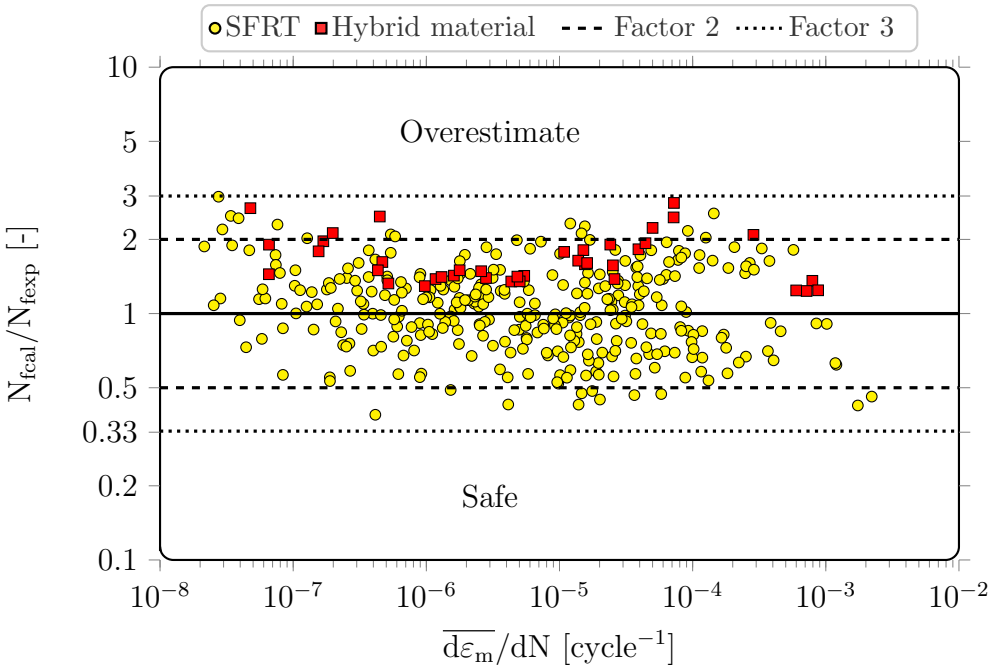

Figure 13: Criterion extrapolation. SFRT tests for 15 different configurations (fibre orientation, water content, positive R_σ and frequency). *Hybrid material* at 0°, $R_\sigma = 0$, 50 % RH.

Test	Material	Test conditions				Test N$_o$.	% data $\left[\frac{1}{n}, n\right]$		Fig.
		RH (%)	θ (°)	f (Hz)	R_σ		n=2	n=3	
LCF	SFRT	50	0, 45, 90	1	0	158	95	100	12
LCF	SFRT	0, 50, 80	0, 45, 90	0.2, 1, 2, 4	0, 0.2, 0.5, 0.8	335	92	100	13
LCF	*Hybrid*	50	0	1	0	39	82	100	13
Creep	SFRT	0, 50, 80	0, 45, 90	-	-	50	94	100	15
Creep + LCF	SFRT	All the conditions listed above				385	93	100	15

Table 3: Criterion precision. Identification made with data related to line one (158 SFRT tests). Percentage of data within a scatter band of factor two and three. For the last two lines the criterion was expressed in the time domain.

as a function of time. Relationship between the number of cycles and time is made through the frequency (Eq. 9). To simplify matters both fatigue mean strain ϵ_m and creep strain ϵ_c are noted ϵ. In time domain *cyclic mean strain rate* criterion is now named as *creep mean strain rate* criterion:

$$\textit{Creep mean strain rate criterion} = \overline{\frac{\mathrm{d}\varepsilon}{\mathrm{d}t}} = f\overline{\frac{\mathrm{d}\varepsilon}{dN}} \tag{12}$$

The relationship to obtain the estimated time to failure is then written as follows:

$$t_{fcal} = B\left(\overline{\frac{\mathrm{d}\varepsilon}{\mathrm{d}t}}\right)^m \tag{13}$$

with:

$$B = A^{-\frac{1}{k}} \textit{ and } m = \frac{1}{k}$$

where B and m are material parameters.

Figure 14 shows the *creep strain rate* criterion evolution as a function of time to failure. Criterion seems applicable to both creep and LCF for the SFRT and the *hybrid material*. The offset between the interpolating line and the *hybrid material* data is attribute to the difference in microstructure and the interface. Creep and fatigue fracture in uniaxial tension under constant stress is described by the Monkman Grant relationship.

$$\overline{\frac{\mathrm{d}\varepsilon}{\mathrm{d}t}} t_f^n = C \tag{14}$$

where $C = A$ and $n = -k$.

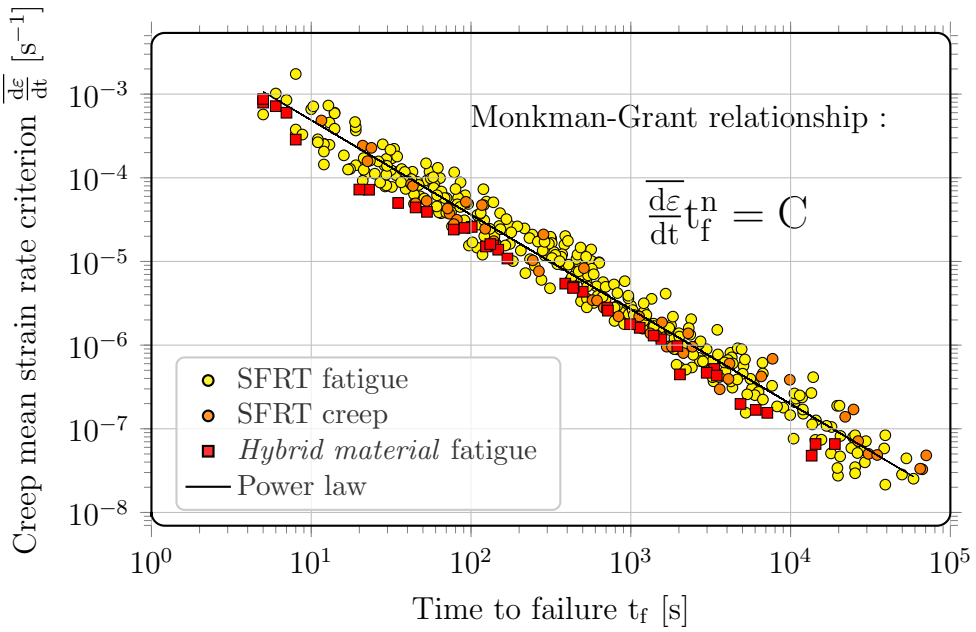

Figure 14: *Creep strain rate* criterion evolution as a function of time to failure. LCF and creep results follow the same Monkman-Grant relation

Figure 15 presents criterion accuracy using the coefficients identified in

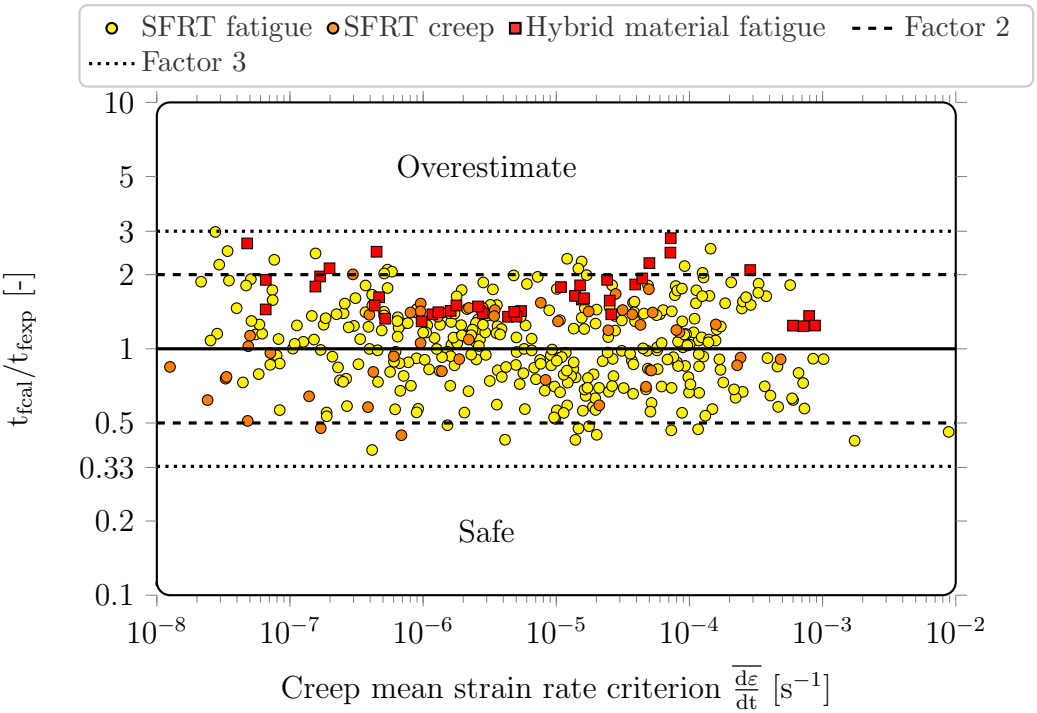

Figure 15: Criterion extrapolation in time domain. SFRT LCF tests for 15 different configurations (fibre orientation, water content, positive R_σ and frequency). SFRT creep test for 7 configurations (fibre orientation and water content) *Hybrid material* LCF tests at 0°, $R_\sigma = 0$, 50 % RH

section 5.1.1. t_{fcal}/t_{fexp} is plotted versus *creep mean strain rate* criterion. t_{fcal} is the estimated lifetime using Eq. 13. t_{fexp} is the experimental lifetime. All test are concerned, i.e. 385 in all. The criterion unifies creep and LCF test with 93 % of estimated lifetimes within a scatter band of factor two and 100 % in factor three (Table 3). These results show the link between creep and fatigue.

6. Conclusions

Creep mean strain rate criterion has been evaluated on a wide range of SFRT LCF and creep tests. LCF results have been obtained for a wide range of load ratios (from 0 to 0.8), frequency (0.5 Hz to 4 Hz), three fibre orientations (0°, 45° and 90°) and three water content conditions (0 % RH, 50 % RH and 80 % RH) at 23 °C. Creep results have been collected for a range three fibre orientations (0°, 45° and 90°) and three water content conditions (0 % RH, 50 % RH and 80 % RH) at 23 °C. LCF *hybrid material* tests have been measured for 0° fibre orientation, $R_\sigma = 0$, 50 % RH and 1 Hz at 23 °C. This *Creep mean strain rate* criterion has only two parameters to identify. Exclusively LCF test database on SFRT at $R_\sigma = 0$, 50 % RH and 1 Hz is used to identify parameters.

The *cyclic mean strain rate* criterion unifies all database results in LCF domain with 92 % of estimated lifetimes within a scatter band of factor two, and 100 % in factor 3. Most of the classic criteria is not able to describe accurately this type of database [14, 15]. The obtained precision is very high compared to the usual fatigue predictions often spanning more than a decade.

The addition of continuous fibres improves fatigue resistance. SFRT have a major influence in *hybrid material* failure. The criterion based on *cyclic creep strain rate* makes it possible to unify the results in the LCF domain for the different microstructure and SFRT test configurations as well as for the *hybrid material* in the direction of the continuous fibres. 100 % of estimated lifetimes for *hybrid material* are within a scatter band of factor three. Despite the SFRT constrained face in hybrid material, the criterion identified on samples with free edges is applicable.

The *creep strain rate* criterion expressed in a time domain unifies the fatigue and creep results through a Monkman-Grant relationship for many influential parameters: frequency, stress ratio, orientation and water content. The criterion unifies creep and LCF test with 93 % of estimated lifetimes within a scatter band of factor two and 100 % in factor three. This result is extremely important because it implies similar damage mechanisms for SFRT in LCF and creep loading, which remains to be verified.

Several perspectives can be considered and Raphael [43] began to address some of them in his thesis. First, understand physical phenomena underlying the *cyclic creep strain rate* evolution (plasticity, visco-elasticity, damage) and the link with *creep strain rate* during creep loading. Second, only uniaxial loading is considered in this paper. An extension to multi-axial loading should be carried out. The last perspective concerns a numerical approach in order to access *creep mean strain rate* criterion. The creep-fatigue relationship seems to be a promising research way for the numerical approach in order to access this criterion at a reduced cost.

7. Acknowledgements

The authors gratefully acknowledge ContiTech AVS France for supporting this work. The authors wish to thank Yvon Tirel and Gilles Lucas for their help in moulding the plates and developing the process, and Romain Ricordel, Zohra Anoune and Aginath Selliah for their help during LCF and creep testing. Finally SG gratefully acknowledges Susan Cameron for her proofreading.

References

[1] A. Bernasconi, P. Davoli, and C. Armanni. Fatigue strength of a clutch pedal made of reprocessed short glass fibre reinforced polyamide. *International Journal of Fatigue*, 32(1):100 – 107, 2010. ISSN 0142-1123. doi: 10.1016/j.ijfatigue.2009.02.001. Fourth International Conference on Fatigue of Composites (ICFC4).

[2] L. Jegou, Y. Marco, V. Le Saux, and S. Calloch. Fast prediction of the Wöhler curve from heat build-up measurements on Short Fiber Reinforced Plastic. *International Journal of Fatigue*, 47:259–267, 2013. ISSN 0142-1123. doi: https://doi.org/10.1016/j.ijfatigue.2012.09.007.

[3] C. M. Sonsino and E. Moosbrugger. Fatigue design of highly loaded short-glass-fibre reinforced polyamide parts in engine compartments. *International Journal of Fatigue*, 30(7):1279–1288, 2008. ISSN 0142-1123. doi: 10.1016/j.ijfatigue.2007.08.017.

[4] S. Gillet, Y. Tirel, F. Canevet, P. Dewailly, L. Laiarinandrasana, S. Joannès, and N. Bedrici. Etude de l'endommagement d'un composite thermoplastique à fibres continues. Colloque MECAMAT Fatigue des Structures et des Matériaux, January 2017.

[5] M. J.W. Kanters, L. F.A. Douven, and P. Savoyat. Fatigue life prediction of injection moulded short glass fiber reinforced plastics. *Procedia Structural Integrity*, 19:698–710, 2019. ISSN 24523216. doi: 10.1016/j.prostr.2019.12.076.

[6] S. Barbouchi, V. Bellenger, A. Tcharkhtchi, Ph. Castaing, and T. Jollivet. Effect of water on the fatigue behaviour of a pa66/glass fiberscomposite material. *Journal of Materials Science*, 42(6):2181–2188, March 2007. ISSN 1573-4803. doi: 10.1007/s10853-006-1011-x.

[7] A. Bernasconi, F. Cosmi, and D. Dreossi. Local anisotropy analysis of injection moulded fibre reinforced polymer composites. *Composites Science and Technology*, 68(12):2574 – 2581, 2008. ISSN 0266-3538. doi: https://doi.org/10.1016/j.compscitech.2008.05.022.

[8] J. J. Horst and J. L. Spoormaker. Mechanisms of fatigue in short glass fiber reinforced polyamide 6. *Polymer Engineering and Science*, 36(22):2718–2726, 1996. doi: 10.1002/pen.10671.

[9] H. Rolland. *Comportement en fatigue et mécanismes d'endommagement du polyamide-66 renforcé par des fibres de verre courtes.* Phd thesis, Ecole nationale supérieure d'arts et métiers - ENSAM, 2017.

[10] J. J. Horst and J. L. Spoormaker. Fatigue fracture mechanism and fractography of short-glassfibre-reinforced polyamide 6. *Journal of Materials Science*, 32:3641–3651, 07 1997. doi: 10.1023/A:1018634530869.

[11] A. Bernasconi and R. Kulin. Effect of frequency upon fatigue strength of a short glass fiber reinforced polyamide 6: A superposition method based on cyclic creep parameters. *Polymer Composites*, 30:154 – 161, 02 2009. doi: 10.1002/pc.20543.

[12] F. R. Larson and J. Miller. Time-Temperature Relationship for Rupture and Creep Stresses. *Transactions of ASME*, 74:765–771, 1952.

[13] E. Seignobos. *Compréhension des mécanismes physiques de fatigue dans le polyamide vierge et renforcé de fibres de verre.* Phd thesis, INSA Lyon, 2009.

[14] I. Raphael, N. Saintier, H. Rolland, G. Robert, and L. Laiarinandrasana. A mixed strain rate and energy based fatigue criterion for short fiber reinforced thermoplastics. *International Journal of Fatigue*, 127:131–143, 2019. doi: 10.1016/j.ijfatigue.2019.06.003.

[15] P. Santharam, Y. Marco, V. Le Saux, M. Le Saux, G. Robert, I. Raoult, C. Guévenoux, D. Taveau, and P. Charrier. Fatigue criteria for short fiber-reinforced thermoplastic validated over various fiber orientations, load ratios and environmental conditions. *International Journal of Fatigue*, 135:105574–1 – 105574–16, 2020. doi: 10.1016/j.ijfatigue.2020.105574.

[16] F.C. Monkman and N.J. Grant. An empirical relationship between rupture life and minimum creep rate in creep-rupture tests. *Proc. American Society of Testing Materials*, 56:593–620, 1956.

[17] G. Sundararajan. The monkman-grant relationship. *Materials Science and Engineering: A*, 112:205 – 214, 1989. ISSN 0921-5093. doi: 10.1016/0921-5093(89)90360-2.

[18] B. K. Choudhary and E. Isaac Samuel. Creep behaviour of modified 9Cr–1Mo ferritic steel. *Journal of Nuclear Materials*, 412(1):82–89, May 2011. ISSN 00223115. doi: 10.1016/j.jnucmat.2011.02.024.

[19] E. M. Haney, F. Dalle, M. Sauzay, L. Vincent, I. Tournié, L. Allais, and B. Fournier. Macroscopic results of long-term creep on a modified 9cr–1mo steel (t91). *Materials Science & Engineering A*, 510-511(Complete):99–103, 2009. doi: 10.1016/j.msea.2008.04.099.

[20] F. Povolo. Comments on the Monkman-Grant and the modified Monkman-Grant relationships. *Journal of Materials Science*, 20(6):2005–2010, June 1985. ISSN 1573-4803. doi: 10.1007/BF01112283.

[21] M. Eftekhari and Ali Fatemi. Creep behavior and modeling of neat, talc-filled, and short glass fiber reinforced thermoplastics. *Composites Part B: Engineering*, 97: 68–83, July 2016. doi: 10.1016/j.compositesb.2016.04.043.

[22] R. M. Guedes. Lifetime predictions of polymer matrix composites under constant or monotonic load. *Composites Part A: Applied Science and Manufacturing*, 37(5): 703 – 715, 2006. ISSN 1359-835X. doi: 10.1016/j.compositesa.2005.07.007.

[23] I. Boumakis, K. Ninčević, J. Vorel, and R. Wan-Wendner. Creep rate based time-to-failure prediction of adhesive anchor systems under sustained load. *Composites Part B: Engineering*, 178:107389, December 2019. ISSN 13598368. doi: 10.1016/j.compositesb.2019.107389.

[24] A. Bernasconi, P. Davoli, A. Basile, and A. Filippi. Effect of fibre orientation on the fatigue behaviour of a short glass fibre reinforced polyamide-6. *International Journal of Fatigue*, 29(2):199–208, 2007. doi: https://doi.org/10.1016/j.ijfatigue.2006.04.001.

[25] B. Klimkeit, Y. Nadot, S. Castagnet, C. Nadot-Martin, C. Dumas, S. Bergamo, C.M. Sonsino, and A. Büter. Multiaxial fatigue life assessment for reinforced polymers. *International Journal of Fatigue*, 33(6):766–780, 2011. doi: https://doi.org/10.1016/j.ijfatigue.2010.12.004.

[26] A. Launay, M. H. Maitournam, Y. Marco, and I. Raoult. Multiaxial fatigue models for short glass fibre reinforced polyamide. Part II: Fatigue life estimation. *International Journal of Fatigue*, 47:390–406, February 2013. doi: 10.1016/j.ijfatigue.2012.09.015.

[27] M. E. Kassner and T. A. Hayes. Creep cavitation in metals. *International Journal of Plasticity*, 19(10):1715–1748, 2003. ISSN 0749-6419. doi: https://doi.org/10.1016/

S0749-6419(02)00111-0.

[28] N. Selles. *Cavitation et rupture du Polyamide 6 sous état de contrainte multiaxial en traction monotone, fluage et fatigue. Dialogue entre imagerie 3D et modélisation par éléments finis.* Phd thesis, École Nationale Supérieure des Mines de Paris, 2017.

[29] R. W. Lang, J. A. Manson, and R. W. Hertzberg. Effect of short glass fibers and particulate fillers on fatigue crack propagation in polyamides. *Polymer Engineering & Science*, 22(15):982–987, 1982. doi: 10.1002/pen.760221513.

[30] A. Megally. *Étude et modélisation de l'orientation de fibres dans des thermoplastiques renforcés.* Phd thesis, École Nationale Supérieure des Mines de Paris, July 2005.

[31] R. Ricordel. Caractérisation du scénario d'endommagement d'un composite à matrice thermoplastique renforcé par des fibres continues. Master thesis, Université de Bretagne Sud, 2018.

[32] G. J. Kettle. Variation of the glass transition temperature of nylon-6 with changing water content. *Polymer*, 18(7):742–743, 1977. ISSN 0032-3861. doi: https://doi.org/10.1016/0032-3861(77)90244-0.

[33] M. Eftekhari and A. Fatemi. Creep-fatigue interaction and thermo-mechanical fatigue behaviors of thermoplastics and their composites. *International Journal of Fatigue*, 91:136 – 148, 2016. ISSN 0142-1123. doi: https://doi.org/10.1016/j.ijfatigue.2016.05.031.

[34] E. Jinen. Creep properties of fatigued short carbon fibre reinforced nylon 6 plastics. *J Mater Sci*, 22(6):1956–1962, June 1987. ISSN 0022-2461, 1573-4803. doi: 10.1007/BF01132923.

[35] D. W. Scott, J. S. Lai, and A.-H. Zureick. Creep behavior of fiber-reinforced polymeric composites: A review of the technical literature. *Journal of Reinforced Plastics and Composites*, 14(6):588–617, 1995. doi: 10.1177/073168449501400603.

[36] M. Eftekhari and A. Fatemi. Tensile, creep and fatigue behaviours of short fibre reinforced polymer composites at elevated temperatures: a literature survey. *Fatigue & Fracture of Engineering Materials & Structures*, 38(12):1395–1418, 2015. doi: 10.1111/ffe.12363.

[37] L. Jégou. *Caractérisation rapide des propriétés en fatigue d'un polymère renforcé par*

des fibres courtes, pour une application automobile. Phd thesis, ENSTA Bretagne, 2012.

[38] A. Launay, Y. Marco, M.H. Maitournam, and I. Raoult. Modelling the influence of temperature and relative humidity on the time-dependent mechanical behaviour of a short glass fibre reinforced polyamide. *Mechanics of Materials*, 56:1–10, January 2013. doi: 10.1016/j.mechmat.2012.08.008.

[39] P.K Mallick and Y. Zhou. Effect of mean stress on the stress-controlled fatigue of a short e-glass fiber reinforced polyamide-6,6. *International Journal of Fatigue*, 26 (9):941–946, 2004. doi: 10.1016/j.ijfatigue.2004.02.003.

[40] M. J. W. Kanters, T. Kurokawa, and L. E. Govaert. Competition between plasticity-controlled and crack-growth controlled failure in static and cyclic fatigue of thermoplastic polymer systems. *Polymer Testing*, 50:101 – 110, 2016. ISSN 0142-9418.

[41] I. Raphael, N. Saintier, G. Robert, J. Béga, and L. Laiarinandrasana. On the role of the spherulitic microstructure in fatigue damage of pure polymer and glass-fiber reinforced semi-crystalline polyamide 6.6. *International Journal of Fatigue*, 126: 44–54, 2019. doi: 10.1016/j.ijfatigue.2019.04.036.

[42] B. Efron and R. Tibshirani. Bootstrap methods for standard errors, confidence intervals, and other measures of statistical accuracy. *Statistical Science*, 1(1):54–75, 1986. ISSN 08834237. doi: 10.1214/ss/1177013815.

[43] I. Raphael. *Fatigue-fluage du Polyamide 6,6 renforcé.* Phd thesis, Ecole nationale supérieure d'arts et métiers - ENSAM, December 2019.

Graphical Abstract

Short-term creep and low cycle fatigue unified criterion for a hybridised composite material

S. Gillet, T. Jacopin, S. Joannès, N. Bedrici, L. Laiarinandrasana

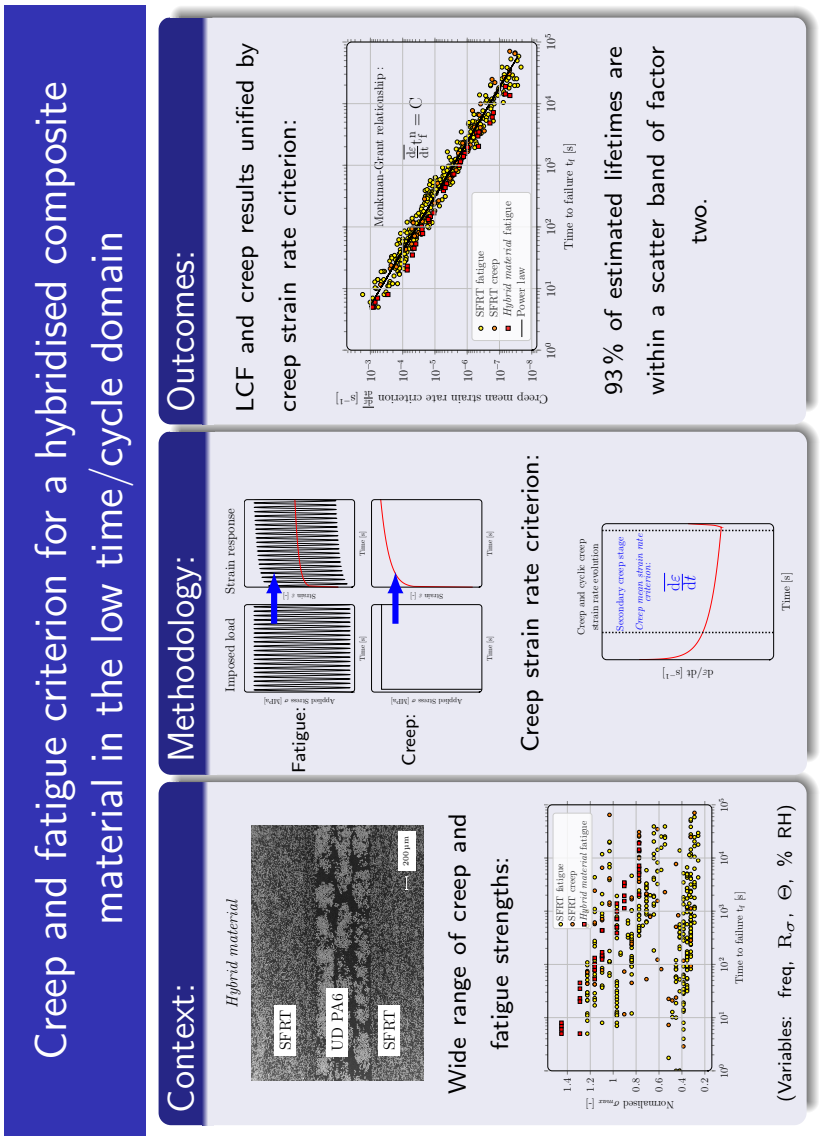

Highlights

Short-term creep and low cycle fatigue unified criterion for a hybridised composite material

S. Gillet, T. Jacopin, S. Joannès, N. Bedrici, L. Laiarinandrasana

- An original *hybrid material* combining short and continuous fibres is presented.
- An unified fatigue criterion based on steady state creep strain rate is proposed.
- The unified criterion shows a link between fatigue and creep phenomena.
- The Monkman-Grant relationship is verified both for creep and low cycle fatigue.